Contributions to OH reactivity from unexplored volatile organic compounds measured by PTR-ToF-MS– A case study in a suburban forest of the Seoul Metropolitan Area during KORUS-AQ 2016

Dianne Sanchez,[1] Roger Seco,[1*] Dasa Gu,[1] Alex Guenther,[1] John Mak,[2] Youngjae Lee,[3] Danbi Kim,[3] Joonyoung Ahn, [3] Don Blake,[4] Scott Herndon,[5] Daun Jeong,[1] John T. Sullivan,[6] Thomas Mcgee,[6] and Saewung Kim[1*]

1. Department of Earth System Science, University of California, Irvine, Irvine CA 92697, U.S.A.

2. School of Marine and Atmospheric Sciences, Stony Brooke University, Stony Brook, NY 11794, U.S.A.

3. National Institute of Environmental Research, Inchoen 22689, South Korea

4. Department of Chemistry, University of California, Irvine, Irvine CA 92697, U.S.A.

5. Aerodyne Research Inc., Billerica MA 01821, U.S.A.

6. NASA Goddard Space Flight Center, Chemistry and Dynamics Laboratory, Greenbelt, MD 20771, U.S.A.

* Now at: Terrestrial Ecology Section, Department of Biology, University of Copenhagen, Copenhagen, Denmark and
Center for Permafrost (CENPERM), Department of Geosciences and Natural Resource Management , University of Copenhagen, Copenhagen, Denmark

Corresponding author: saewung.kim@uci.edu, tel 1-949-824-4531

To be submitted to Atmospheric Chemistry and Physics

Abstract

We report OH reactivity observations by a chemical ionization mass spectrometer – comparative reactivity method (CIMS-CRM) instrument in a suburban forest of the Seoul Metropolitan Area (SMA) during Korea US Air Quality Study (KORUS-AQ 2016) from mid-May to mid-June of 2016. A comprehensive observational suite was deployed to quantify reactive trace gases inside of the forest canopy including a high-resolution proton transfer reaction time of flight mass spectrometer (PTR-ToF-MS). An average OH reactivity of 30.7 ± 5.1 s^{-1} was observed, while the OH reactivity calculated from CO, NO + NO_2 (NO_x), ozone (O_3), sulfur dioxide (SO_2), and 14 volatile organic compounds (VOCs) was 11.8 ± 1.0 s^{-1}. An analysis of 346 peaks from the PTR-ToF-MS accounted for an additional 6.0 ± 2.2 s^{-1} of the total measured OH reactivity, leaving 42.0 % missing OH reactivity. A series of analyses indicates that the missing OH reactivity most likely comes from VOC oxidation products of both biogenic and anthropogenic origin.

1. Introduction

Total OH reactivity (s^{-1}), the inverse of OH lifetime, is a measure of the total amount of reactive trace gases in the atmosphere in the scale of reactivity, which allow us to quantitatively evaluate our ability to constrain trace gases by comparing measurements of total OH reactivity with the OH reactivity calculated from a speciated reactive gas measurement dataset. The fraction of observed OH reactivity that cannot be reconciled by calculated OH reactivity is known as "missing OH reactivity" (Di Carlo et al., 2004;Goldstein and Galbally, 2007;Yang et al., 2016). A substantial amount of missing OH reactivity has consistently been reported in forest environments (30 - 80%). Di Carlo et al. (2004) conducted a study in a mixed forest near Pellston, Michigan where they reported missing OH reactivity (~ 30 %) larger than observational uncertainty. The authors concluded that the missing sources of reactivity were primary biogenic volatile organic compound (biogenic VOC, BVOC) emissions, as the degree of missing OH reactivity followed the temperature dependence of terpenoid emissions. In a boreal forest in Hyytiälä, Finland, Sinha et al. (2010) report a similar result with observed trace gases that account for only 50% of the measured OH reactivity. They argued that oxidation products of BVOCs alone could not account for the missing OH reactivity. Thus, they also concluded that primary emissions were more likely to be the source of missing OH reactivity and they further suggest that this could be the result of the contribution of small amounts of many reactive gases. Follow up studies (Nolscher et al., 2012;Praplan et al., 2019) at the same site have presented a consistent conclusion. Nolscher et al. (2012) observed the highest level of missing OH reactivity during a heat wave episode, possibly inducing a stress emission response from the local forest. A comprehensive analysis by Praplan et al. (2019) using a long-term observation dataset and a

72 photochemical model framework with the Master Chemical Mechanism illustrates that the model
73 simulated oxidation compound contribution can only contribute 7 % of missing OH reactivity.
74 On the other hand, some studies have attributed the sources of the missing OH reactivity
75 to unmeasured oxidation products of well-characterized BVOCs. Edwards et al. (2013)
76 measured OH reactivity in a pristine tropical forest in the Sabah region of Borneo during the
77 Oxidant and Particle Photochemical Processes (OP3) field campaign (Hewitt et al., 2010). This
78 study implemented the Master Chemical Mechanism (MCMv3.2) (Saunders et al., 2003;Jenkin
79 et al., 1997) into a box model framework to quantify potential contributions from unmeasured
80 oxidation products. The model was constrained with VOCs such as isoprene, monoterpenes, and
81 alkanes and alkenes and other observed trace gases such as NO + NO_2 (NO_x) and ozone (O_3).
82 The authors reported that the model simulated oxygenated VOCs (OVOCs) could contribute
83 47.1% of the calculated OH reactivity – surpassing the contribution from isoprene, the primary
84 emission of this ecosystem. It is notable that 30% of observed OH reactivity could not be
85 accounted for by the box model simulations. After examining the comprehensive observational
86 suite of VOCs, the authors determined that the most significant missing sources of OH reactivity
87 were likely secondary multifunctional carbon compounds rather than primary BVOC emissions.
88 Hansen et al. (2014) suggested that their observed missing OH reactivity were likely from
89 unmeasured oxidation products during the Community Atmosphere-Biosphere INteraction
90 EXperiment (CABINEX 2009) in Michigan. This notion was also consistent with findings
91 reported by Kim et al. (2011) who measured OH reactivity of branch enclosures from four
92 representative tree species in the forest canopy during the CABINEX study. They reconciled
93 most of the measured OH reactivity of four representative tree species with well-known BVOCs,
94 such as isoprene and monoterpenes. Finally, Nakashima et al. (2014) reported that 29.5% OH

reactivity could not be reconciled by the speciated trace gas dataset during the Bio-hydro-atmosphere interactions of Energy, Aerosols, Carbon, H_2O, Organics and Nitrogen-Southern Rocky Mountain 2008 (BEACHON-SMR08) field campaign (Ortega et al., 2014). The campaign took place at the Manitou Experimental Forest (MEF) in Colorado, a ponderosa pine plantation dominated by primary BVOC emissions of 2-methyl-3-butene-2-ol (232-MBO) and monoterpenes (Ortega et al., 2014). The authors also reported that the missing OH reactivity was likely from BVOC oxidation products. In the same context, Kim et al. (2010) conducted PTR-MS mass spectrum analysis for both ambient air and branch enclosures at the MEF site. They reported more conspicuous unidentified signals on PTR-MS mass spectra in the ambient samples than those from branch enclosure samples at this site.

During the Southern Oxidant and Aerosol Study (SOAS) in 2013, Kaiser et al. (2016) used a comprehensive suite of VOC measurements at an isoprene dominant forest site in the southeastern US to examine the role of the OVOC species in missing reactive carbon. The authors used MCMv3.2 embedded in the University of Washington Chemical Box Model (UWCM) to compare OH reactivity from model-generated OVOCs to OH reactivity from measurements of OVOCs. There was no significant discrepancy between the average measured and calculated OH reactivity including observed trace gases and model calculated oxidation products of VOCs. However, it was noted that a small portion (1 s^{-1}) of observed OH reactivity could not be reconciled by the model calculation. As this fraction was not correlated to isoprene oxidation products, it was suggested that the missing OH reactivity may be due to unmeasured primary emissions. One caveat of this analysis pointed out by the authors was that the concentrations of the modeled first-generation isoprene oxidation products (e.g. MVK, MACR, isoprene hydroxy hydroperoxides (ISOPOOH), isoprene nitrates (ISOPN), and hydroperoxy

aldehydes (HPALD)) were significantly overpredicted in the afternoon. Consequently, the uncertainty of the model calculation is likely to be much higher for the multi-generation oxidation products and their contributions to the OH reactivity contributions. This result highlights the uncertainty in relying solely on box-model results to assess OH reactivity. This *status quo* urges us to take a convergent approach by effectively integrating observational results from novel instrumentation and model outcomes.

This study examines the OH reactivity observations at Taehwa Research Forest (TRF) supersite from 15 May 2016 to 7 June 2016 during the Korea United States Air Quality Study 2016 (KORUS-AQ 2016) campaign. TRF (37 18' 19.08" N 127 19' 7.12" E, 162 m altitude) is operated by Seoul National University and located in Gwangju in the Gyunggi Province in South Korea (Kim et al., 2013b). The site is about 35 km southeast from the center of Seoul and borders the greater Seoul Metropolitan Area (SMA) with its population of 25.6 million. This geographical proximity to SMA results in a significant level of anthropogenic influence, particularly in elevated NO_x (Kim et al., 2016). Additionally, occasional pollution transport events occur at regional scales. Previous studies at the site have consistently highlighted the importance of BVOC photochemistry at TRF (Kim et al., 2016;Kim et al., 2013a;Kim et al., 2015). Isoprene and monoterpenes are the dominant OH sinks at the site among observed VOCs. The elevated NO_X accelerates the photochemical processing of VOCs (Kim et al., 2015). Thus, this site is an ideal natural laboratory to study contributions towards total OH reactivity from primary trace gas emissions from both natural and anthropogenic processes and their oxidation products. This motivated us to deploy a high-resolution proton transfer reaction time-of-flight mass spectrometer (PTR-ToF-MS) to quantify trace amounts of VOCs with unknown molecular structures by taking advantage of the universal sensitivity of hydronium ion chemistry towards

reactive VOCs (Graus et al., 2010;Jordan et al., 2009a). Therefore, we intend to observationally constrain the contributions of conventionally unidentified or unmeasured VOCs towards OH reactivity.

2. Methods

2.1. Field Site

The Taehwa Research Forest is a Korean pine (*Pinus koraiensis*) plantation (300 m × 300 m) surrounded by a deciduous forest dominated by oak trees (Kim et al., 2013b). A flux tower (40 m height) at the center of TRF has air-sampling inlets at multiple heights (4 m, 8 m 12 m, and 16 m) below the canopy top (20 m). Each inlet consists of Teflon tubing (3/8" OD) with ~ 1 second of residence time. The trace gas dataset including VOCs presented is the average of concentrations measured at the inlets inside of the canopy as previous studies illustrate that there is no substantial vertical VOC gradients inside of the canopy (within 3 %, Kim et al. (2013b)). An air-conditioned instrument shack located at the base of the flux tower housed the PTR-ToF-MS for VOC measurements, a mini tunable infrared laser direct absorption spectroscopy (mini-TILDAS) instrument for HCHO, methane, and methanol measurements, and analyzers for carbon monoxide (CO), sulfur dioxide (SO_2), ozone (O_3), and meteorological measurements. The OH reactivity and NO_x analyzers were located in another nearby air-conditioned shack (3 m apart) and sampled air through an extended Teflon inlet line of 4 m (¼" OD) from the ground with a flow rate of 4 sLpm resulting in a 0.5 second residence time. The height of the ambient air intake was 3.5 m. The analytical characteristics of the instrumentation suite are summarized in Table 1. A ceilometer backscattering characterized boundary layer vertical structure at the site. The ceilometer analysis described by Sullivan et al. (2019) reveals the diurnal boundary layer

height evolution, indicating a maximum in the afternoon around 1-3 km and a minimum in the early morning below 500 m.

2.2.OH Reactivity Measurements

A chemical ionization mass spectrometer – comparative reactivity method (CIMS-CRM) instrument was used to measure OH reactivity. The UCI CIMS-CRM system includes a chemical ionization mass spectrometer with a hydronium reagent ion. The CRM method measures total OH reactivity by quantifying the relative loss of pyrrole, a highly reactive gas ($k_{OH+\ pyrrole}$ = 1.07 × 10^{-10} cm^3 $molecule^{-1}$ s^{-1} at 298 K (Dillon et al., 2012)) that is rarely found in the atmosphere (Sinha et al., 2008b). Nitrogen gas flows through a bubbler full of ultrapure liquid chromatography mass spectrometer (LC-MS) grade water to produce water vapor. The water vapor then flows into a glass reactor where it is photolyzed into OH radicals by a mercury lamp (Pen-Ray® Light Source P/N 90-0012-01). The measurement uncertainty is 16.7% (1σ) with a limit of detection of 4.5 s^{-1} over 2 minutes (3σ).

The UCI CIMS-CRM instrument has been deployed on multiple occasions, including the Megacity Air Pollution Study (MAPS)-Seoul 2015 campaign that incorporated previous measurements at the TRF ground site during September 2015 (Sanchez et al., 2018;Kim et al., 2016). During the SOAS 2013 campaign, an ambient OH reactivity intercomparison study was conducted with laser induced fluorescence (LIF) system (Sanchez et al., 2018). The instrument intercomparison showed that the OH reactivity measurements from the CRM and LIF instruments generally agreed within the analytical uncertainty. An average of 16% difference between the techniques was noted in the late afternoons where the CRM measurements were lower than those from LIF. As discussed in Sanchez et al. (2018), this is likely caused by the

187 difference in sampling strategies, as the CRM measurements relied on a lengthy Teflon inlet (15
188 m) while the LIF directly sampled air at the top of a walk up tower. As mentioned above, at TRF
189 we used a shorter inlet line to minimize residence time and avoid inlet line loss.
190 An extensive intercomparison study was conducted by Fuchs et al. (2017) with various
191 OH reactivity measurement techniques that highlighted potential analytical artifacts in the CRM
192 technique. These artifacts have all been examined and preventive measures have been
193 implemented in the UCI CIMS-CRM system deployed at TRF. This included a laboratory-built
194 catalytic converter (Pt-wool at 350 °C) that minimized the interferences due to changes in air to
195 prevent the interference from the difference in humidity for the zero air characterizations.
196 Hansen et al. (2015) illustrated that NO_X may be generated from the catalytic converter. To
197 prevent potential NO_X interferences, they used a scrubber with Purafil and activated charcoal,
198 which will modulate the humidity in the sample. Our approach to this type of interference has
199 been to determine the maximum NO level, noticeably interfering with the calibration regression
200 line shown in Sanchez et al. (2018). Laboratory tests indicate that the statistical agreement
201 started to veer off when the NO level is 5 ppb in 1 σ of the linear regression between instrument
202 response (unitless) and OH reactivity (s^{-1}) as the slope for the calibration curve has changed from
203 0.238 to 0.246. In addition, Kim et al. (2016) achieved an OH reactivity budget closure in high
204 NO_2 condition, which implies no significant interferences from NO_2. However, in response to the
205 Fuchs et al. (2017) observation that various CRM configurations suffer from different levels of
206 NO_X interferences, we plan to conduct more systematic NO_X interference tests to more
207 accurately characterize this system. In conclusion, it is possible that our reported OH reactivity
208 may systematically underestimate ambient total OH reactivity as much as ambient OH reactivity
209 coming from NO_2.

We consistently kept the pyrrole to OH ratio at 3:1 and so did not achieve a pseudo first order relationship. Even in the field environment with various relative humidity, we have not observed noticeable changes in this ratio as we flow bulk humidified nitrogen (150 standard cc per minute) to the reactor with the total flow of 240 cc, which result in dampening the temporal ambient relative humidity variations. Therefore, we performed multi-point calibrations (5 s^{-1} to 30 s^{-1}) with a propene mixture using a NIST traceable gas standard (AirLiquide LLC, 0.847 ppm) during the field campaign to avoid any circumstances where the pseudo first-order reaction regime is not established. Detailed calibration procedures for the OH reactivity system including laboratory multi-component calibration results can be found in Sanchez et al. (2018).

In addition, Fuchs et al. (2017) also described a potential interference from ambient O_3 in some CRM systems. In the 2015 field campaigns conducted in Seoul South Korea (Kim et al., 2016), we conducted a standard addition experiment for the propene standard for additional ~ 30 s^{-1} in two different ozone environment 65 ppb and 123 ppb. The outcome illustrates an agreement between two additions within the analytical uncertainty although a systematic laboratory study will warrant an accurate uncertainty assessment from ozone. Again, as the CRM method is a relatively new technique, one should keep in mind that the future studies may find potential artifacts that we do not report in this study.

2.3.PTR-ToF-MS Measurements

A high-resolution PTR-TOF-MS (Ionicon Analytik GmbH) (de Gouw and Warneke, 2007b), (Jordan et al., 2009b) was deployed at the TRF site. The instrument was operated with a drift tube temperature of 60 ˚C, 560 V drift voltage, and 2.27 mbar drift tube to maintain E/N of 126 Td. Background checks were manually conducted about three times a day for a 10-minute

duration by scrubbing the ambient air through a catalytic convertor (Pt-wool maintained at 350°C). The detectable peaks from the ambient spectra were assessed by subtracting the background spectrum. The instrument was calibrated with a gas mixture manufactured by Apel-Riemer Environmental Inc. The mixture contains ~ 1 ppmv of acetaldehyde, acetone, isoprene, methyl vinyl ketone, methacrolein, benzene, methly ethyl ketone, toluene, o-xylene, and α-pinene. This standard mixture was only used for the PTR-ToF-MS calibration and not the CRM-CIMS calibration. The concentration of the compounds were assessed in the Blake Lab at University of California, Irvine, who also conducted the airborne VOC analysis using whole air samples during the KORUS-AQ campaign on the NASA DC-8 (Colman et al., 2001).

A mass range of m/z 40 to m/z 267 was analyzed from the recorded PTR-ToF-MS mass spectra. An automatic mass scale calibration was conducted every 5 minutes on the data averaged over 30 seconds. The raw PTR-ToF-MS data were processed using the PTRwid software described by Holzinger (2015). We normalized the mass peaks by 10^6 reagent ion counts (H_3O^+). As the majority of the VOC mass peaks could not be directly calibrated, we determined the VOC sensitivities using equation 1 (Eq 1). This method has been employed by a number of previous studies such as Cappellin et al. (2012). The benzene calibration factor was used to calculate mixing ratios by applying its proton transfer reaction rate coefficient (k_{benzene}) and sensitivity (ncps ppb^{-1}) for the available compounds. The application of this equation can be justified since PTRwid provides the mass discrimination corrected counts as a final computational product.

$$ppb_{VOC} = ncps_{VOC} \times \frac{k_{benzene}}{k_{VOC}} \times \frac{1}{11.94\ ncps\ ppb^{-1}} \qquad \text{Eq. 1}$$

where, 11.94 ncps ppb-1 is the assessed sensitivity of benzene.

256 ppb_{VOC} is the mixing ratio of an analyte.

257 $ncps_{VOC}$ is the mass discrimination corrected normalized count for an analyte.

258 $k_{benzene}$ is the proton transfer reaction rate constant for benzene.

259 k_{VOC} is the proton transfer reaction rate constant for an analyte.

260

261 For the mass peaks where specific proton transfer reaction rates were unavailable, we
262 estimated the mixing ratios by applying a proton transfer reaction rate coefficient (k_{H3O+}) of 3.00
263 $\times 10^{-9}$ cm^3 s^{-1}, the default value for PTRwid calculations. The spectra had a limit of detection of
264 tens of ppt for a 30 second average. The calibrated compounds had a range of detection limits as
265 low as 3.7 ppt for α-pinene and as high as 48 ppt for toluene.

266

267 **2.4. *OH Reactivity Calculation***

268 OH reactivity was calculated from the concentrations of all the compounds observed by
269 the instrumental suite described in Table 1. The original data can be found in the KORUS-AQ
270 2016 data archive at https://korus-aq.larc.nasa.gov/. A total of 360 mass peaks measured by the
271 PTR-ToF-MS were analyzed above the background (3 σ or above) to assess their contribution to
272 the calculated OH reactivity. Fourteen of the mass peaks were identified as VOCs commonly
273 reported for PTR-MS measurements (Table 1), leaving 346 unidentified peaks. These remaining
274 mass peaks were grouped into three categories in order to estimate their possible OH reactivity
275 contribution.

276 Category I (81 peaks) included mass peaks for which the PTRwid software calculated a
277 molecular formula. OH reaction rate coefficients for the individual peaks were obtained from the
278 National Institute for Standards and Technology (NIST) Webbook library. As the only

279 information we have is the molecular composition, we identified multiple isomers with different
280 functional groups and thus different reactivity. We have extensively reviewed previous
281 publications (Williams et al., 2001;De Gouw et al., 2003;de Gouw and Warneke, 2007a;Jordan et
282 al., 2009a;Ruuskanen et al., 2011;Muller et al., 2012;Koss et al., 2017a) identifying ambient
283 VOCs using PTR-MS with both quadrupole and time-of-flight systems to identify possible
284 compounds. For example, for the m/z of 75.043, there are four possible compounds including
285 hydroxy acetone, propionic acid, methyl acetate, and ethyl formate. We used the median reaction
286 constant for the set of possible compounds. The detailed description of the OH reaction constant
287 determination process for the Category I peaks is described in Sanchez (2019). If the information
288 was unavailable from the NIST Webbook database, a structure-reactivity relationship described
289 by Kwok and Atkinson (1995) was applied to obtain reaction rate coefficients. This is an
290 empirical calculation system to estimate k_{OH} based upon the number of carbons and the
291 functional groups of given VOCs. The framework is able to calculate k_{OH} within a factor of two
292 according to a thorough assessments presented in Kwok and Atkinson (1995). However, the
293 authors discourage the application of the framework to compounds that were not examined in the
294 study such as halogenated compounds. Although halogenated compounds are not included in this
295 study, one should be aware of a potentially significant uncertainty.
296 Category II (28 peaks) included mass peaks for which the PTRwid software could not
297 assess an exact molecular composition due to uncertainty in the data processing system.
298 Nonetheless, this group of compounds illustrated a positive correlation (R^2 = 0.19 to 0.88) with
299 either anthropogenic (benzene, toluene) or biogenic (MVK+MACR and monoterpenes) VOCs.
300 Category II compounds are further grouped into subcategories corresponding to these two main
301 VOC sources. OH reaction rate constants (k_{OH}) were estimated with equations based on the

relationship between the *m/z* and the k_{OH} of compounds in Table 1 (Figure S1). More specifically, we assume that k_{OH} is linearly correlated with m/z. To apply this linear relationship, the compounds with known k_{OH} were grouped into 5 *m/z* bins and the average k_{OH} of each bin was calculated. The green triangles represent 5 *m/z* binned averages from these compounds plotted with their respective average k_{OH}. This approach can be justified by the fact that the reaction constants of VOCs towards OH tend to increase as a function of molecular mass within functional groups (Kwok and Atkinson, 1995;Atkinson, 1987). The y-intercepts of the linear regressions were assessed using the k_{OH} values of the biogenic or anthropogenic compounds and their masses.

Category III (237 peaks) included mass peaks with very low mixing ratios (average = 4.8 ppt ±19.5 ppt) that were above the limit of detection. We applied a k_{OH} corresponding to the dark green best-fit line in Figure S1 to these peaks. The y-intercept of the dark green line was based on that of acetaldehyde, as it was the lowest mass compound used for the OH reactivity calculations in this study.

There are two components that need to be considered for the assessment of uncertainty associated with calculated OH reactivity: the concentration and the reaction constants with OH. The uncertainty of the observed trace gases is in the range of 5 % to 20 % as shown in Table 1 and is associated with the rate constants from laboratory experiments (Atkinson et al., 2006). Combining 15 % uncertainty from reaction constants and 13.5 % from trace gas observations results in 20 % of uncertainty in calculated OH reactivity. This should be considered as a conservative estimate as most VOC concentrations and associated rate constants are empirically estimated.

3. Results and Discussion

An average OH reactivity of 30.7 ± 5.1 s^{-1} was observed from 15 May – 7 June 2016 (Figure 1). This was within the range of OH reactivity observed in urban regions (10 - 33 s^{-1}). (Kovacs et al., 2003;Ren et al., 2003;Sinha et al., 2008a;Dolgorouky et al., 2012;Whalley et al., 2016;Kim et al., 2016;Yang et al., 2017) and in the range of previously reported observations and model calculations at the TRF site (~15 - 35 s^{-1}) (Kim et al., 2016;Kim et al., 2015). The total calculated OH reactivity of 11.8 ± 1.0 s^{-1} from the measured compounds in Table 1 resulted in 63.3% missing OH reactivity. However, an additional OH reactivity of 6.0 ± 2.2 s^{-1} was further calculated from the reactivity of the VOCs in Categories I – III. The contribution lowered the missing OH reactivity level to 42% of the measured OH reactivity. Kim et al. (2016) had previously measured an average OH reactivity of 16.5 s^{-1} at TRF during the MAPS-Seoul campaign from 1 September – 15 September 2015, a substantially lower level then what we report during this springtime study. Although small alkanes and alkenes such as ethane, ethene, propane and propene were not observed on the site, we utilized the dataset from the NASA DC-8 that flew at 700 m above the site, which indicates that their contribution was consistently small (~ 0.7 s^{-1} in average). In this suburban forest, we do not think there is any substantial emission sources of these relatively long-lived VOCs.

The difference can be attributed to the notably higher reactive trace gas loadings during KORUS-AQ compared to the TRF measurements during MAPS-Seoul. The NO_x, benzene, and toluene concentrations were 3 times higher during KORUS-AQ and CO was 1.4 times higher (Figure S2). Although the average isoprene concentrations were similar between the two campaigns, MVK and MACR concentrations during KORUS-AQ were ~3 times higher, illustrating a higher oxidative environment. There was a persistently high MVK+MACR to

348 isoprene ratio of 1.8 during the KORUS-AQ campaign at TRF. This ratio was similar to the
349 value reported during the summer in a moderately polluted forest in the Pearl River Delta that
350 was attributed to a strong atmospheric oxidation capacity (Gong et al., 2018). The missing OH
351 reactivity during KORUS-AQ was generally much higher than levels reported during urban
352 observations (up to 50% missing OH reactivity) (Kovacs et al., 2003;Ren et al., 2003;Sinha et
353 al., 2008a;Dolgorouky et al., 2012;Whalley et al., 2016;Kim et al., 2016;Yang et al., 2017) and
354 within the range of previously reported values in forest regions where as much as 80% missing
355 OH reactivity has been reported (Kim et al., 2016;Di Carlo et al., 2004;Nolscher et al.,
356 2012;Edwards et al., 2013;Nolscher et al., 2016;Ramasamy et al., 2018;Nakashima et al., 2014).
357 Figure 2 shows the diurnal average of measured, calculated, and missing OH reactivity
358 from 15 May – 7 June 2016. Isoprene was the largest contributor to VOC OH reactivity in the
359 afternoon and the early evening (36% of the calculated OH reactivity in the evening), consistent
360 with the previous studies conducted in this site (Kim et al., 2016;Kim et al., 2013b;Kim et al.,
361 2015). Among all the trace gases, the largest average contributor to the calculated OH reactivity
362 was NO_x, which contributed 18.2% (5.6 s^{-1}) to the measured OH reactivity. The NO_x
363 contribution to OH reactivity is higher during the morning and evening rush hours and at a
364 minimum in the afternoon, which has been reported consistently in previous reports conducted
365 near megacities (Kovacs et al., 2003;Mao et al., 2010;Dolgorouky et al., 2012;Ren et al.,
366 2003;Shirley et al., 2006). Enhanced OH reactivity during the morning or night and minimum
367 OH reactivity during the afternoon have been reported in urban areas (Kovacs et al., 2003;Ren et
368 al., 2006;Shirley et al., 2006;Dolgorouky et al., 2012;Mao et al., 2010;Whalley et al., 2016). On
369 the other hand, strong light-sensitive biogenic emissions (e.g. isoprene) result in a maximum
370 observed OH reactivity in the afternoon in forested regions (Ren et al., 2006;Sinha et al.,

371 2012;Edwards et al., 2013;Hansen et al., 2014;Zannoni et al., 2017;Nolscher et al., 2016) . One
372 exception is an OH reactivity observation conducted in Hyytiälä, a forested site that has low
373 isoprene levels, by Sinha et al. (2010). They attributed a flat diurnal OH reactivity variation to
374 the interplay between high daytime emissions and low nighttime boundary layer height. In urban
375 environments, it is mostly anthropogenic trace gases such as aromatics and OVOCs that
376 contribute to OH reactivity. These compounds have a longer lifetime compared to the diurnal
377 boundary layer evolution. This leads to the accumulation of such compounds in the shallow
378 boundary layer during the night. On the other hand, strong emissions of reactive BVOCs in
379 deciduous forest regions enhance OH reactivity during the daytime but then quickly react away.
380 Very subtle diurnal differences observed in this study (Figure 2), therefore, can be understood as
381 the competitive influences of both anthropogenic and biogenic compounds to the OH reactivity.
382 As described in detail in Sullivan et al. (2019) and Jeong et al. (2019), a strong regional
383 stagnation episode occurred during the KORUS-AQ campaign between May 17 – 23. Later, the
384 Korean Peninsula was affected by a period of continental pollution outflow between May 28 and
385 June 1. The diurnal averages of the two periods and their calculated OH reactivity are presented
386 in Figure 3. It is notable that there is very little difference in the observed OH reactivity between
387 the two distinct periods in terms of the amount of OH reactivity and its diurnal pattern (Figure 4).
388 Furthermore, no significant variance of the different classes of reactive gases such as criteria air
389 pollutants (CO, NO_x, O_3, and SO_2), mostly contributed by NO_X, OVOCs (acetone, acetaldehyde,
390 formaldehyde, methylglyoxal, methanol, methyl ethyl ketone), aromatics (benzene, toluene,
391 xylenes, styrene, benzaldehyde, trimethylbenzenes), and BVOCs (isoprene, monoterpenes,
392 sesquiterpenes, MVK+MACR) was observed during the different periods (Figure 5). These
393 different classes of reactive gases generally differed by less than 10% during the two periods

394 from the overall campaign. This observation shows that the presence of reactive gases is mostly
395 controlled by relatively short-lived compounds determined by local emissions and their oxidation
396 products.

397 The diurnal variation behavior of each chemical class reflects the chemical lifetime of the
398 compounds (e.g. aromatics vs BVOCs). The calculated OH reactivity from OVOCs does not
399 show a strong diurnal variation. This reflects the fact that OVOCs are mostly generated or
400 emitted during the daytime and their lifetime is generally longer than their precursors, which
401 allows nocturnal accumulation due to the absence of OH. The differences in the diurnal variation
402 of different classes of reactive gases can also be used to interpret the origin of the compounds in
403 Categories I-III as presented in Figure 6. The diurnal variations of Category I resemble those of
404 relatively long-lived chemical species with a distinct nocturnal accumulation pattern. This
405 diurnal pattern has been previously reported for both anthropogenic VOCs such as toluene and
406 benzene and temperature dependent monoterpenes such as α-pinene. It is notable that the diurnal
407 pattern is enhanced during the stagnation period during early morning hours. This enhancement
408 is also seen in the aromatic trace gases particularly during the stagnation period (Figure 5b).

409 Indeed, there are both biogenic and anthropogenic contributions towards the Category I
410 compounds, which contribute an average of 3.8 s^{-1} to the OH reactivity assessment, the largest
411 amount among the three categories (Figure 6a). The largest contributors to Category I, which
412 appear to be from a mixture of biogenic and anthropogenic sources, include *m/z* 89.060, 101.06,
413 and 101.096, and they contributed 0.3 s^{-1}, 0.2 s^{-1}, and 0.2 s^{-1}, respectively. The m/z 89.060 had a
414 molecular formula of $C_4H_8O_2H^+$ and was correlated to the anthropogenic compounds such as
415 benzene and toluene. The *m/z* 101.06 peak had the molecular formula of $C_5H_8O_2H^+$ and had a
416 diurnal variation similar to that of MVK + MACR. This mass peak has been previously

identified in laboratory (Zhao et al., 2004) and field (Williams et al., 2001) studies as the C_5 hydroxy carbonyl, an isoprene oxidation product. Results from an indoor chamber photooxidation experiment conducted by Lee et al. (2006) showed that *m/z* 101 is a common fragment of unidentified oxidation products of monoterpenes, sesquiterpenes, and isoprene. Lee et al. (2006) also reported that this mass peak also composed over 5% of the fragments of unidentified α- humulene and linalool oxidation products. The molecular formula of this peak is $C_6H_{12}OH^+$, and it has been identified in previous studies as C_6 carbonyls (Koss et al., 2017b) or hexanal (Brilli et al., 2014;Rinne et al., 2005). Furthermore, *m/z* 99.044 and 113.023 were also among the highest contributors to Category I and were correlated with MVK and MACR. The *m/z* 99 was previously reported to be a fragment ion of unidentified terpene oxidation products in a chamber experiment (Lee et al., 2006). The *m/z* 113 was observed by a PTR-MS in a Ponderosa pine forest in central California by Holzinger et al. (2005). In this case, it was formed within the canopy from the rapid oxidation of terpinolene, myrcene, and α-terpinene. Furthermore, *m/z* 113 was observed to come from the photooxidation and ozonolyis of multiple terpenes in two indoor chamber studies by Lee et al. (2006). The m/z 113 composed over 5% of the oxidation product fragments of myrcene and verbenone. Finally, m/z 83.085 had the molecular formula of $C_6H_{11}^+$ and was correlated to benzene. Multiple studies have identified this peak as cyclohexane, methyl-cyclopentane, or methylcyclohexane, typically found in areas rich in oil and gas (Koss et al., 2017b;Gueneron et al., 2015;Yuan et al., 2014). In summary, both the gross diurnal pattern and the individual peak analyses consistently illustrates that both anthropogenic and biogenic compounds comprise Category I, the largest contributor to the previously unexplored compounds in the PTR-ToF-MS spectrum at this research site.

Category II contributed an average of 0.3 s^{-1} to the calculated OH reactivity, the lowest amount for the three Categories (Figure 6b). The compounds in category II appear to correlate to either BVOCs or acetone, depending on the time period. In Figure 6b, the maximum during the transport period is enhanced to about 0.2 s^{-1} higher than the overall campaign and shifted about 3 hours later to ~4:00 PM. The OH reactivity calculated from Category II is strongly correlated to MVK + MACR (r^2 = 0.82) during this period as well. On the other hand, during the stagnation period the average OH reactivity from Category II correlates more strongly with acetone (r^2 = 0.62) than with MVK +MACR (r^2 = 0.28). In fact, six of the highest contributors to Category II (Figure 6b) are more strongly correlated to acetone (r^2 > 0.40) during the stagnation period compared to the transport period. The sources of acetone can be either biogenic or anthropogenic. Biogenic sources include direct emissions from plants or their oxidation products and plant decay (Jacob et al., 2002;Seco et al., 2007). Anthropogenic sources of acetone include vehicular emissions, solvent use, and the oxidation of other anthropogenic VOCs (Jacob et al., 2002). Therefore, this illustrates that the compounds in Category II also have a complex source profile of both biogenic and anthropogenic origin.

Category III contributed 1.9 s^{-1} to the calculated OH reactivity (Figure 6c). The six highest contributors out of 236 mass peaks contributed a total of 0.43 s^{-1} of the calculated OH reactivity. Overall, Category III compounds had no strong correlations to isoprene, MVK+MACR, benzene, or toluene during either the stagnation or transport periods. However, Category III compounds were highly correlated to methylglyoxal (r^2 = 0.85, 0.82, and 0.78 for the stagnation, transport, and overall period, respectively), one of the measured OVOCs. A global modeling study illustrated that methylglyoxal is mainly produced from isoprene oxidation processes and the second most important source is acetone oxidation (Fu et al., 2008). In

addition, aromatics and alkenes are also known to produce methylglyoxal through atmospheric oxidation processes (Henry et al., 2012). As TRF is a high aromatics and high isoprene environment, the source profile of methyl glyoxal in the region is likely complex, which can be applied to interpret the source of the Category III compounds.

Overall, the OH reactivity estimates from Categories I – III contributed an average of 6.0 $\pm$ 2.2 s^{-1} to the calculated OH reactivity. In summary, there is consistency that both anthropogenic and the biogenic contributions need to be further studied in the PTR-ToF-MS spectrum. Furthermore, by adding this additional signal from Category I, II, and III, VOC contribution to calculated OH reactivity (11.0 s^{-1}) becomes larger than that (6.8 s^{-1}) from criteria air pollutants (CO, NO_x, SO_2 and O_3). This should be considered when evaluating ozone production regimes (Kim et al., 2018).

Even with the inclusion of the additional peaks to the calculated OH reactivity, we still find a missing OH reactivity of 42%. Thus, it is important to investigate the origin of this missing fraction. A correlation can be observed between missing OH reactivity in percentage and OH reactivity from NO_X (R2 = 0.5, Figure 7 A) but not between OH reactivity from NO_x and absolute missing OH reactivity (s^{-1}) (R2 = 0.2, Figure 7 B). This leads us to speculate that there is a consistent presence of unquantified trace gases, likely oxidation products of both anthropogenic and biogenic VOCs as we explored the origin of the unexplored peaks causing missing OH reactivity. In other words, NO_x is relatively well measured with a highly pronounced temporal variation that determines the percentage of missing OH reactivity.

Finally, unaccounted for uncertainty associated with the reaction rate constant estimations described in the method section should be also further explored. For example, to reconcile the averaged missing OH reactivity during the day (10 s^{-1}), it requires ~ 60 ppm of

485 methane but only ~ 4 ppb of isoprene. This clearly demonstrates the importance of rate constant
486 estimation. Indeed, if we apply the reaction rate constant of isoprene with OH (k_{OH} = 1 × 10^{-10}
487 cm^3 $molecule^{-1}$ s^{-1}at 298 K) to Category II and Category III compounds, then the observed OH
488 reactivity is fully reconciled (Figure S3). Proton ion chemistry may have an intrinsic limitation to
489 quantify highly oxidized OVOCs. Moreover, due to the different inlet configurations for OH
490 reactivity and VOC observations, their contributions towards observed and calculated OH
491 reactivity may not have been consistently evaluated (e.g. Sanchez et al. (2018)). Therefore, a
492 comprehensive analysis along with a dataset from other instrumentation is necessary towards
493 reconciling missing OH reactivity with observational constraints. Finally, it is highly plausible
494 that we may double count for fragmented molecules in the mass spectrum. Although it would not
495 affect concentration evaluation as the intensity of ion signals from the fragmented molecules
496 would be fully accounted for by adding parent ion and fragmented ion signals, the OH reactivity
497 calculated from the fragmented ions is susceptible to underestimation from the assumption that
498 k_{OH} positively correlates with molecular masses.
499
500 ***4. Summary***
501 We present OH reactivity observations at a suburban forest site during the KORUS-AQ field
502 campaign. A comprehensive trace gas dataset including 14 VOCs quantified by PTR-ToF-MS is
503 used to calculate OH reactivity, which only accounts for 36.7 % of the averaged observed OH
504 reactivity.
505 This study presents a detailed methodology for retrieving OH reactivity contributions from
506 all of the peaks of the PTR-ToF-MS mass spectrum. This decreases the amount of missing OH
507 reactivity as the majority of them have not been accounted towards calculated OH reactivity in

previous studies. First, we converted the raw signals to concentrations using a constant proton transfer reaction rate (3×10^{-9} cm^3 s^{-1}). Then, we grouped the previously unaccounted peaks into three categories to estimate reaction constants for each compound. The contributions of the unaccounted peaks in the mass spectrum account for a calculated OH reactivity of ~ 6 s^{-1}, which decreases missing OH reactivity from 63.3 % to 42.0 %. It is noteworthy that the diurnal variations of observed OH reactivity and calculated OH reactivity from the various groups of trace gases does not have a high variability during the field campaign even though there were several synoptic meteorological configuration changes. This suggests that the reactive trace gas loading is mostly determined by local emission and oxidation processes not influenced by the synoptic meteorological conditions.

In conclusion, this study highlights PTR-ToF-MS as a tool for observationally constraining missing OH reactivity. Further study is required particularly towards characterizing proton reaction rate constants and reaction constants with OH for the many unknown compounds detected on PTR-ToF-MS. In addition, other mass spectrometry techniques, such as nitrate or iodine ion chemistry systems, should be utilized in future studies to complement the PTR technique, which is sensitive to volatile to semi volatile VOCs, to quantify lower volatility compounds and comprehensively constrain OH reactivity contributions from VOCs.

Acknowledgements

This study is supported by NASA (NNX15AT90G) and NIER. We highly appreciate NASA ESPO for logistical support. Taehwa Research Forest is operated by College of Agriculture and Life Sciences at Seoul National University. S. Kim would like to acknowledge a funding support

from Brain Pool Program of National Research Foundation Korea (NRF) Funded by the Ministry of Science ICT (# 2020H1D3A2A01060699).

Data Availability

Data is available at: https://korus-aq.larc.nasa.gov/

References

Atkinson, R.: A Structure-Activity Relationship for the Estimation of Rate Constants for the Gas-Phase Reactions of Oh Radicals with Organic-Compounds, International Journal of Chemical Kinetics, 19, 799-828, DOI 10.1002/kin.550190903, 1987.

Atkinson, R., Baulch, D. L., Cox, R. A., Crowley, J. N., Hampson, R. F., Hynes, R. G., Jenkin, M. E., Rossi, M. J., and Troe, J.: Evaluated kinetic and photochemical data for atmospheric chemistry: Volume II - gas phase reactions of organic species, Atmospheric Chemistry and Physics, 6, 3625-4055, 2006.

Brilli, F., Gioli, B., Ciccioli, P., Zona, D., Loreto, F., Janssens, I. A., and Ceulemans, R.: Proton Transfer Reaction Time-of-Flight Mass Spectrometric (PTR-TOF-MS) determination of volatile organic compounds (VOCs) emitted from a biomass fire developed under stable nocturnal conditions, Atmospheric Environment, 97, 54-67, 10.1016/j.atmosenv.2014.08.007, 2014.

Cappellin, L., Karl, T., Probst, M., Ismailova, K., Winkler, P. M., Soukoulis, C., Aprea, E., Mark, T. D., Gasperi, F., and Biasioli, F.: On quantitative determination of volatile organic compound concentrations using proton transfer reaction Time-of-Flight Mass Spectrometry, Environment Science & Technology, 46, 2012.

Colman, J. J., Swanson, A. L., Meinardi, S., Sive, B. C., Blake, D. R., and Rowland, F. S.: Description of the analysis of a wide range of volatile organic compounds in whole air samples collected during PEM-Tropics A and B, Analytical Chemistry, 73, 3723-3731, 2001.

De Gouw, J., Goldan, P., Warneke, C., Kuster, W., Roberts, J. M., Marchewka, M., Bertman, S. B., Pszenny, A., and Keene, W.: Validation of proton transfer reaction-mass spectrometry (PTR-MS) measurements of gas phase organic compounds in the atmosphere during the New England Air Quality Study (NEAQS) in 2002, Journal of Geophysical Research, 108, 4682 doi:4610.1029/2003JD003863, 2003.

de Gouw, J., and Warneke, C.: Measurements of volatile organic compounds in the earths atmosphere using proton-transfer-reaction mass spectrometry, Mass Spectrom Rev, 26, 223-257, 2007a.

de Gouw, J., and Warneke, C.: Measurements of volatile organic compounds in the earth's atmosphere using proton-transfer-reaction mass spectrometry, Mass Spectrom Rev, 26, 223-257, 10.1002/mas.20119, 2007b.

Di Carlo, P., Brune, W. H., Martinez, M., Harder, H., Lesher, R., Ren, X. R., Thornberry, T., Carroll, M. A., Young, V., Shepson, P. B., Riemer, D., Apel, E., and Campbell, C.: Missing OH reactivity in a forest: Evidence for unknown reactive biogenic VOCs, Science, 304, 722-725, Doi 10.1126/Science.1094392, 2004.

Dillon, T. J., Tucceri, M. E., Dulitz, K., Horowitz, A., Vereecken, L., and Crowley, J. N.: Reaction of Hydroxyl Radicals with C4H5N (Pyrrole): Temperature and Pressure Dependent Rate Coefficients, Journal of Physical Chemistry A, 116, 6051-6058, 10.1021/jp211241x, 2012.

Dolgorouky, C., Gros, V., Sarda-Esteve, R., Sinha, V., Williams, J., Marchand, N., Sauvage, S., Poulain, L., Sciare, J., and Bonsang, B.: Total OH reactivity measurements in Paris during the 2010 MEGAPOLI winter campaign, Atmospheric Chemistry and Physics, 12, 9593-9612, Doi 10.5194/Acp-12-9593-2012, 2012.

Edwards, P. M., Evans, M. J., Furneaux, K. L., Hopkins, J., Ingham, T., Jones, C., Lee, J. D., Lewis, A. C., Moller, S. J., Stone, D., Whalley, L. K., and Heard, D. E.: OH reactivity in a South East Asian tropical rainforest during the Oxidant and Particle Photochemical Processes (OP3) project, Atmospheric Chemistry and Physics, 13, 9497-9514, Doi 10.5194/Acp-13-9497-2013, 2013.

Fu, T. M., Jacob, D. J., Wittrock, F., Burrows, J. P., Vrekoussis, M., and Henze, D. K.: Global budgets of atmospheric glyoxal and methylglyoxal, and implications for formation of secondary organic aerosols, Journal of Geophysical Research-Atmospheres, 113, 2008.

Fuchs, H., Novelli, A., Rolletter, M., Hofzumahaus, A., Pfannerstill, E. Y., Kessel, S., Edtbauer, A., Williams, J., Michoud, V., Dusanter, S., Locoge, N., Zannoni, N., Gros, V., Truong, F., Sarda-Esteve, R., Cryer, D. R., Brumby, C. A., Whalley, L. K., Stone, D., Seakins, P. W., Heard, D. E., Schoemaecker, C., Blocquet, M., Coudert, S., Batut, S., Fittschen, C., Thames, A. B., Brune, W. H., Ernest, C., Harder, H., Muller, J. B. A., Elste, T., Kubistin, D., Andres, S., Bohn, B., Hohaus, T., Holland, F., Li, X., Rohrer, F., Kiendler-Scharr, A., Tillmann, R., Wegener, R., Yu, Z. J., Zou, Q., and Wahner, A.: Comparison of OH reactivity measurements in the atmospheric simulation chamber SAPHIR, Atmospheric Measurement Techniques, 10, 4023-4053, 2017.

Goldstein, A. H., and Galbally, I. E.: Known and unexplored organic constituents in the earth's atmosphere, Environmental Science & Technology, 41, 1514-1521, 2007.

Gong, D. C., Wang, H., Zhang, S. Y., Wang, Y., Liu, S. C., Guo, H., Shao, M., He, C. R., Chen, D. H., He, L. Y., Zhou, L., Morawska, L., Zhang, Y. H., and Wang, B. G.: Low-level summertime isoprene observed at a forested mountaintop site in southern China: implications for strong regional atmospheric oxidative capacity, Atmospheric Chemistry and Physics, 18, 14417-14432, 10.5194/acp-18-14417-2018, 2018.

Graus, M., Muller, M., and Hansel, A.: High Resolution PTR-TOF: Quantification and Formula Confirmation of VOC in Real Time, J Am Soc Mass Spectr, 21, 1037-1044, 2010.

Gueneron, M., Erickson, M. H., VanderSchelden, G. S., and Jobson, B. T.: PTR-MS fragmentation patterns of gasoline hydrocarbons, International Journal of Mass Spectrometry, 379, 97-109, 10.1016/j.ijms.2015.01.001, 2015.

Hansen, R. F., Griffith, S. M., Dusanter, S., Rickly, P. S., Stevens, P. S., Bertman, S. B., Carroll, M. A., Erickson, M. H., Flynn, J. H., Grossberg, N., Jobson, B. T., Lefer, B. L., and

614 Wallace, H. W.: Measurements of total hydroxyl radical reactivity during CABINEX
615 2009-Part 1: field measurements, Atmospheric Chemistry and Physics, 14, 2923-2937,
616 10.5194/acp-14-2923-2014, 2014.
617 Hansen, R. F., Blocquet, M., Schoemaecker, C., Leonardis, T., Locoge, N., Fittschen, C.,
618 Hanoune, B., Stevens, P. S., Sinha, V., and Dusanter, S.: Intercomparison of the
619 comparative reactivity method (CRM) and pump-probe technique for measuring total OH
620 reactivity in an urban environment, Atmospheric Measurement Techniques, 8, 4243-
621 4264, 10.5194/amt-8-4243-2015, 2015.
622 Henry, S. B., Kammrath, A., and Keutsch, F. N.: Quantification of gas-phase glyoxal and
623 methylglyoxal via the Laser-Induced Phosphorescence of (methyl)GLyOxal
624 Spectrometry (LIPGLOS) Method, Atmospheric Measurement Techniques, 5, 181-192,
625 10.5194/amt-5-181-2012, 2012.
626 Herndon, S. C., Jayne, J. T., Zahniser, M. S., Worsnop, D. R., Knighton, B., Alwine, E., Lamb,
627 B. K., Zavala, M., Nelson, D. D., McManus, J. B., Shorter, J. H., Canagaratna, M. R.,
628 Onasch, T. B., and Kolb, C. E.: Characterization of urban pollutant emission fluxes and
629 ambient concentration distributions using a mobile laboratory with rapid response
630 instrumentation, Faraday Discussions, 130, 327-339, 10.1039/b500411j, 2005.
631 Hewitt, C. N., Lee, J. D., MacKenzie, A. R., Barkley, M. P., Carslaw, N., Carver, G. D.,
632 Chappell, N. A., Coe, H., Collier, C., Commane, R., Davies, F., Davison, B., Di Carlo, P.,
633 Di Marco, C. F., Dorsey, J. R., Edwards, P. M., Evans, M. J., Fowler, D., Furneaux, K.
634 L., Gallagher, M., Guenther, A., Heard, D. E., Helfter, C., Hopkins, J., Ingham, T., Irwin,
635 M., Jones, C., Karunaharan, A., Langford, B., Lewis, A. C., Lim, S. F., MacDonald, S.
636 M., Mahajan, A. S., Malpass, S., McFiggans, G., Mills, G., Misztal, P., Moller, S.,
637 Monks, P. S., Nemitz, E., Nicolas-Perea, V., Oetjen, H., Oram, D. E., Palmer, P. I.,
638 Phillips, G. J., Pike, R., Plane, J. M. C., Pugh, T., Pyle, J. A., Reeves, C. E., Robinson, N.
639 H., Stewart, D., Stone, D., Whalley, L. K., and Yin, X.: Overview: oxidant and particle
640 photochemical processes above a south-east Asian tropical rainforest (the OP3 project):
641 introduction, rationale, location characteristics and tools, Atmospheric Chemistry and
642 Physics, 10, 169-199, 10.5194/acp-10-169-2010, 2010.
643 Holzinger, R., Lee, A., Paw, K. T., and Goldstein, A. H.: Observations of oxidation products
644 above a forest imply biogenic emissions of very reactive compounds, Atmospheric
645 Chemistry and Physics, 5, 67-75, DOI 10.5194/acp-5-67-2005, 2005.
646 Holzinger, R.: PTRwid: A new widget tool for processing PTR-TOF-MS data, Atmospheric
647 Measurement Techniques, 8, 3903-3922, 10.5194/amt-8-3903-2015, 2015.
648 Jacob, D. J., Field, B. D., Jin, E. M., Bey, I., Li, Q. B., Logan, J. A., Yantosca, R. M., and Singh,
649 H. B.: Atmospheric budget of acetone, Journal of Geophysical Research-Atmospheres,
650 107, Artn 4100
651 10.1029/2001jd000694, 2002.
652 Jenkin, M. E., Saunders, S. M., and Pilling, M. J.: The tropospheric degradation of volatile
653 organic compounds: A protocol for mechanism development, Atmospheric Environment,
654 31, 81-104, Doi 10.1016/S1352-2310(96)00105-7, 1997.
655 Jeong, D., Seco, R., Gu, D., Lee, Y. R. O., Nault, B. A., Knote, C. J., Mcgee, T., Sullivan, J. T.,
656 Jimenez, J. L., Campuzano-Jost, P., Blake, D. R., Sanchez, D., Guenther, A. B., Tanner,
657 D., Huey, L. G., Long, R., Anderson, B. E., Hall, S. R., Ullmann, K., Shin, H. J.,
658 Herndon, S. C., Lee, Y. A. E., Kim, D., Ahn, O. O. Y., and Kim, S.: Integration of
659 airborne and ground observations of nitryl chloride in the Seoul metropolitan area and the

implications on regional oxidation capacity during KORUS-AQ 2016, Atmospheric Chemistry and Physics, 19, 12779-12795, 10.5194/acp-19-12779-2019, 2019.
Jordan, A., Haidacher, S., Hanel, G., Hartungen, E., Mark, L., Seehauser, H., Schottkowsky, R., Sulzer, P., and Mark, T. D.: A high resolution and high sensitivity proton-transfer-reaction time-of-flight mass spectrometer (PTR-TOF-MS), International Journal of Mass Spectrometry, 286, 122-128, 2009a.
Jordan, A., Haidacher, S., Hanel, G., Hartungen, E., Märk, L., Seehauser, H., Schottkowsky, R., Sulzer, P., and Märk, T. D.: A high resolution and high sensitivity proton-transfer-reaction time-of-flight mass spectrometer (PTR-TOF-MS), Int J Mass Spectrom, 286, 122-128, http://dx.doi.org/10.1016/j.ijms.2009.07.005, 2009b.
Kaiser, J., Skog, K. M., Baumann, K., Bertman, S. B., Brown, S. B., Brune, W. H., Crounse, J. D., de Gouw, J. A., Edgerton, E. S., Feiner, P. A., Goldstein, A. H., Koss, A., Misztal, P. K., Nguyen, T. B., Olson, K. F., St Clair, J. M., Teng, A. P., Toma, S., Wennberg, P. O., Wild, R. J., Zhang, L., and Keutsch, F. N.: Speciation of OH reactivity above the canopy of an isoprene-dominated forest, Atmospheric Chemistry and Physics, 16, 9349-9359, 10.5194/acp-16-9349-2016, 2016.
Kim, S., Karl, T., Guenther, A., Tyndall, G., Orlando, J., Harley, P., Rasmussen, R., and Apel, E.: Emissions and ambient distributions of Biogenic Volatile Organic Compounds (BVOC) in a ponderosa pine ecosystem: interpretation of PTR-MS mass spectra, Atmospheric Chemistry and Physics, 10, 1759-1771, 2010.
Kim, S., Guenther, A., Karl, T., and Greenberg, J.: Contributions of primary and secondary biogenic VOC tototal OH reactivity during the CABINEX (Community Atmosphere-Biosphere INteractions Experiments)-09 field campaign, Atmospheric Chemistry and Physics, 11, 8613-8623, 10.5194/acp-11-8613-2011, 2011.
Kim, S., Wolfe, G. M., Mauldin, L., Cantrell, C., Guenther, A., Karl, T., Turnipseed, A., Greenberg, J., Hall, S. R., Ullmann, K., Apel, E., Hornbrook, R., Kajii, Y., Nakashima, Y., Keutsch, F. N., DiGangi, J. P., Henry, S. B., Kaser, L., Schnitzhofer, R., Graus, M., Hansel, A., Zheng, W., and Flocke, F. F.: Evaluation of HOx sources and cycling using measurement-constrained model calculations in a 2-methyl-3-butene-2-ol (MBO) and monoterpene (MT) dominated ecosystem, Atmospheric Chemistry and Physics, 13, 2031-2044, Doi 10.5194/Acp-13-2031-2013, 2013a.
Kim, S., Kim, S. Y., Lee, M., Shim, H., Wolfe, G. M., Guenther, A. B., He, A., Hong, Y., and Han, J.: Impact of isoprene and HONO chemistry on ozone and OVOC formation in a semirural South Korean forest, Atmospheric Chemistry and Physics, 15, 4357-4371, Doi 10.5194/Acp-15-4357-2015, 2015.
Kim, S., Sanchez, D., Wang, M. D., Seco, R., Jeong, D., Hughes, S., Barletta, B., Blake, D. R., Jung, J., Kim, D., Lee, G., Lee, M., Ahn, J., Lee, S.-D., Cho, G., Sung, M.-Y., Lee, Y.-H., Kim, D. B., Kim, Y., Woo, J. H., Jo, D., Park, R., Park, J. H., Hong, Y.-D., and Hong, J.-H.: OH Reactivity in Urban and Suburban regions in Seoul, South Korea-An East Asia megacity in a rapid transition, Faraday Discussions, DOI:10.1039/C5FD00230C, DOI:10.1039/C1035FD00230C, 2016.
Kim, S., Jeong, D., Sanchez, D., Wang, M., Seco, R., Blake, D., Meinardi, S., Barletta, B., Hughes, S., Jung, J., Kim, D., Lee, G., Lee, M., Ahn, J., Lee, S.-D., Cho, G., Sung, M.-Y., Lee, Y.-H., and Park, R.: The Controlling Factors of Photochemical Ozone Production in Seoul, South Korea, Aerosol Air Qual Res, 18, 2253-2261, 10.4209/aaqr.2017.11.0452, 2018.

706 Kim, S. Y., Jiang, X. Y., Lee, M., Turnipseed, A., Guenther, A., Kim, J. C., Lee, S. J., and Kim,
707 S.: Impact of biogenic volatile organic compounds on ozone production at the Taehwa
708 Research Forest near Seoul, South Korea, Atmospheric Environment, 70, 447-453, Doi
709 10.1016/J.Atmosenv.2012.11.005, 2013b.
710 Koss, A., Yuan, B., Warneke, C., Gilman, J. B., Lerner, B. M., Veres, P. R., Peischl, J.,
711 Eilerman, S., Wild, R., Brown, S. S., Thompson, C. R., Ryerson, T., Hanisco, T., Wolfe,
712 G. M., Clair, J. M. S., Thayer, M., Keutsch, F. N., Murphy, S., and de Gouw, J.:
713 Observations of VOC emissions and photochemical products over US oil- and gas-
714 producing regions using high-resolution H3O+ CIMS (PTR-ToF-MS), Atmos. Meas.
715 Tech., 10, 2941-2968, 10.5194/amt-10-2941-2017, 2017a.
716 Koss, A., Yuan, B., Warneke, C., Gilman, J. B., Lerner, B. M., Veres, P. R., Peischl, J.,
717 Eilerman, S., Wild, R., Brown, S. S., Thompson, C. R., Ryerson, T., Hanisco, T., Wolfe,
718 G. M., Clair, J. M. S., Thayer, M., Keutsch, F. N., Murphy, S., and de Gouw, J.:
719 Observations of VOC emissions and photochemical products over US oil- and gas-
720 producing regions using high-resolution H3O+ CIMS (PTR-ToF-MS), Atmospheric
721 Measurement Techniques, 10, 2941-2968, 10.5194/amt-10-2941-2017, 2017b.
722 Kovacs, T. A., Brune, W. H., Harder, H., Martinez, M., Simpas, J. B., Frost, G. J., Williams, E.,
723 Jobson, T., Stroud, C., Young, V., Fried, A., and Wert, B.: Direct measurements of urban
724 OH reactivity during Nashville SOS in summer 1999, Journal of Environmental
725 Monitoring, 5, 68-74, 10.1039/b204339d, 2003.
726 Kwok, E. S. C., and Atkinson, R.: Estimation of Hydroxyl Radical Reaction-Rate Constants for
727 Gas-Phase Organic-Compounds Using a Structure-Reactivity Relationship - an Update,
728 Atmospheric Environment, 29, 1685-1695, Doi 10.1016/1352-2310(95)00069-B, 1995.
729 Lee, A., Goldstein, A. H., Kroll, J. H., Ng, N. L., Varutbangkul, V., Flagan, R. C., and Seinfeld,
730 J. H.: Gas-phase products and secondary aerosol yields from the photooxidation of 16
731 different terpenes, Journal of Geophysical Research-Atmospheres, 111, Artn D17305
732 10.1029/2006jd007050, 2006.
733 Mao, J. Q., Ren, X. R., Chen, S. A., Brune, W. H., Chen, Z., Martinez, M., Harder, H., Lefer, B.,
734 Rappengluck, B., Flynn, J., and Leuchner, M.: Atmospheric oxidation capacity in the
735 summer of Houston 2006: Comparison with summer measurements in other metropolitan
736 studies, Atmospheric Environment, 44, 4107-4115, 10.1016/j.atmosenv.2009.01.013,
737 2010.
738 Muller, M., Graus, M., Wisthaler, A., Hansel, A., Metzger, A., Dommen, J., and Baltensperger,
739 U.: Analysis of high mass resolution PTR-TOF mass spectra from 1,3,5-trimethylbenzene
740 (TMB) environmental chamber experiments, Atmospheric Chemistry and Physics, 12,
741 829-843, 10.5194/acp-12-829-2012, 2012.
742 Nakashima, Y., Kato, S., Greenberg, J., Harley, P., Karl, T., Turnipseed, A., Apel, E., Guenther,
743 A., Smith, J., and Kajii, Y.: Total OH reactivity measurements in ambient air in a
744 southern Rocky mountain ponderosa pine forest during BEACHON-SRM08 summer
745 campaign, Atmospheric Environment, 85, 1-8, 2014.
746 Nolscher, A. C., Williams, J., Sinha, V., Custer, T., Song, W., Johnson, A. M., Axinte, R.,
747 Bozem, H., Fischer, H., Pouvesle, N., Phillips, G., Crowley, J. N., Rantala, P., Rinne, J.,
748 Kulmala, M., Gonzales, D., Valverde-Canossa, J., Vogel, A., Hoffmann, T., Ouwersloot,
749 H. G., de Arellano, J. V. G., and Lelieveld, J.: Summertime total OH reactivity
750 measurements from boreal forest during HUMPPA-COPEC 2010, Atmospheric
751 Chemistry and Physics, 12, 8257-8270, Doi 10.5194/Acp-12-8257-2012, 2012.

Nolscher, A. C., Yanez-Serrano, A. M., Wolff, S., de Araujo, A. C., Lavric, J. V., Kesselmeier, J., and Williams, J.: Unexpected seasonality in quantity and composition of Amazon rainforest air reactivity, Nature Communications, 7, ARTN 10383 10.1038/ncomms10383, 2016.

Ortega, J., Turnipseed, A., Guenther, A. B., Karl, T. G., Day, D. A., Gochis, D., Huffman, J. A., Prenni, A. J., Levin, E. J. T., Kreidenweis, S. M., DeMott, P. J., Tobo, Y., Patton, E. G., Hodzic, A., Cui, Y. Y., Harley, P. C., Hornbrook, R. S., Apel, E. C., Monson, R. K., Eller, A. S. D., Greenberg, J. P., Barth, M. C., Campuzano-Jost, P., Palm, B. B., Jimenez, J. L., Aiken, A. C., Dubey, M. K., Geron, C., Offenberg, J., Ryan, M. G., Fornwalt, P. J., Pryor, S. C., Keutsch, F. N., DiGangi, J. P., Chan, A. W. H., Goldstein, A. H., Wolfe, G. M., Kim, S., Kaser, L., Schnitzhofer, R., Hansel, A., Cantrell, C. A., Mauldin, R. L., and Smith, J. N.: Overview of the Manitou Experimental Forest Observatory: site description and selected science results from 2008 to 2013, Atmospheric Chemistry and Physics, 14, 6345-6367, 10.5194/acp-14-6345-2014, 2014.

Praplan, A. P., Tykka, T., Chen, D., Boy, M., Taipale, D., Vakkari, V., Zhou, P. T., Petaja, T., and Hellen, H.: Long-term total OH reactivity measurements in a boreal forest, Atmospheric Chemistry and Physics, 19, 14431-14453, 10.5194/acp-19-14431-2019, 2019.

Ramasamy, S., Nagai, Y., Takeuchi, N., Yamasaki, S., Shojia, K., Ida, A., Jones, C., Tsurumaru, H., Suzuki, Y., Yoshino, A., Shimada, K., Nakashima, Y., Kato, S., Hatakeyama, S., Matsuda, K., and Kajii, Y.: Comprehensive measurements of atmospheric OH reactivity and trace species within a suburban forest near Tokyo during AQUAS-TAMA campaign, Atmospheric Environment, 184, 166-176, 10.1016/j.atmosenv.2018.04.035, 2018.

Ren, X. R., Harder, H., Martinez, M., Lesher, R. L., Oliger, A., Shirley, T., Adams, J., Simpas, J. B., and Brune, W. H.: HOx concentrations and OH reactivity observations in New York City during PMTACS-NY2001, Atmospheric Environment, 37, 3627-3637, 10.1016/S1352-2310(03)00460-6, 2003.

Ren, X. R., Brune, W. H., Oliger, A., Metcalf, A. R., Simpas, J. B., Shirley, T., Schwab, J. J., Bai, C. H., Roychowdhury, U., Li, Y. Q., Cai, C. X., Demerjian, K. L., He, Y., Zhou, X. L., Gao, H. L., and Hou, J.: OH, HO2, and OH reactivity during the PMTACS-NY Whiteface Mountain 2002 campaign: Observations and model comparison, Journal of Geophysical Research-Atmospheres, 111, Artn D10s03 10.1029/2005jd006126, 2006.

Rinne, J., Ruuskanen, T. M., Reissell, A., Taipale, R., Hakola, H., and Kulmala, M.: On-line PTR-MS measurements of atmospheric concentrations of volatile organic compounds in a European boreal forest ecosystem, Boreal Environ Res, 10, 425-436, 2005.

Ruuskanen, T. M., Mueller, M., Schnitzhofer, R., Karl, T., Graus, M., Bamberger, I., Hortnagl, L., Brilli, F., Wohlfahrt, G., and Hansel, A.: Eddy covariance VOC emission and deposition fluxes above grassland using PTR-TOF, Atmospheric Chemistry and Physics, 11, 611-625, 2011.

Sanchez, D., Jeong, D., Seco, R., Wrangham, I., Park, J.-H., Brune, W. H., Koss, A., Gilman, J., de Gouw, J., Misztal, P., Goldstein, A., Baumann, K., Wennberg, P. O., Keutsch, F. N., Guenther, A., and Kim, S.: Intercomparison of OH and OH reactivity measurements in a high isoprene and low NO environment during the Southern Oxidant and Aerosol Study (SOAS), Atmospheric Environment, 174, 227-236, 10.1016/j.atmosenv.2017.10.056, 2018.

Sanchez, D.: Towards the closure of OH reactivity and volatile organic compound budget in the troposphere using in situ observations, Ph. D., Deaprtment of Earth System Science, University of California, Irvine, 2019.
Saunders, S. M., Jenkin, M. E., Derwent, R. G., and Pilling, M. J.: Protocol for the development of the Master Chemical Mechanism, MCM v3 (Part A): tropospheric degradation of non-aromatic volatile organic compounds, Atmospheric Chemistry and Physics, 3, 161-180, 2003.
Seco, R., Penuelas, J., and Filella, I.: Short-chain oxygenated VOCs: Emission and uptake by plants and atmospheric sources, sinks, and concentrations, Atmospheric Environment, 41, 2477-2499, 10.1016/j.atmosenv.2006.11.029, 2007.
Shirley, T. R., Brune, W. H., Ren, X., Mao, J., Lesher, R., Cardenas, B., Volkamer, R., Molina, L. T., Molina, M. J., Lamb, B., Velasco, E., Jobson, T., and Alexander, M.: Atmospheric oxidation in the Mexico City Metropolitan Area (MCMA) during April 2003, Atmospheric Chemistry and Physics, 6, 2753-2765, DOI 10.5194/acp-6-2753-2006, 2006.
Sinha, V., Williams, J., Crowley, J. N., and Lelieveld, J.: The comparative reactivity method - a new tool to measure total OH reactivity in ambient air, Atmospheric Chemistry and Physics, 8, 2213-2227, 2008a.
Sinha, V., Williams, J., Crowley, J. N., and Lelieveld, J.: The Comparative Reactivity Method – a new tool to measure total OH Reactivity in ambient air, Atmos. Chem. Phys., 8, 2213-2227, 10.5194/acp-8-2213-2008, 2008b.
Sinha, V., Williams, J., Lelieveld, J., Ruuskanen, T. M., Kajos, M. K., Patokoski, J., Hellen, H., Hakola, H., Mogensen, D., Boy, M., Rinne, J., and Kulmala, M.: OH Reactivity Measurements within a Boreal Forest: Evidence for Unknown Reactive Emissions, Environmental Science & Technology, 44, 6614-6620, Doi 10.1021/Es101780b, 2010.
Sinha, V., Williams, J., Diesch, J. M., Drewnick, F., Martinez, M., Harder, H., Regelin, E., Kubistin, D., Bozem, H., Hosaynali-Beygi, Z., Fischer, H., Andres-Hernandez, M. D., Kartal, D., Adame, J. A., and Lelieveld, J.: Constraints on instantaneous ozone production rates and regimes during DOMINO derived using in-situ OH reactivity measurements, Atmospheric Chemistry and Physics, 12, 7269-7283, Doi 10.5194/Acp-12-7269-2012, 2012.
Sullivan, J. T., McGee, T. J., Stauffer, R. M., Thompson, A. M., Weinheimer, A., Knote, C., Janz, S., Wisthaler, A., Long, R., Szykman, J., Park, J., Lee, Y., Kim, S., Jeong, D., Sanchez, D., Twigg, L., Sumnicht, G., Knepp, T., and Schroeder, J. R.: Taehwa Research Forest: a receptor site for severe domestic pollution events in Korea during 2016, Atmospheric Chemistry and Physics, 19, 5051-5067, 10.5194/acp-19-5051-2019, 2019.
Whalley, L. K., Stone, D., Bandy, B., Dunmore, R., Hamilton, J. F., Hopkins, J., Lee, J. D., Lewis, A. C., and Heard, D. E.: Atmospheric OH reactivity in central London: observations, model predictions and estimates of in situ ozone production, Atmospheric Chemistry and Physics, 16, 2109-2122, 10.5194/acp-16-2109-2016, 2016.
Williams, J., Poschl, U., Crutzen, P. J., Hansel, A., Holzinger, R., Warneke, C., Lindinger, W., and Lelieveld, J.: An atmospheric chemistry interpretation of mass scans obtained from a proton transfer mass spectrometer flown over the tropical rainforest of Surinam, Journal of Atmospheric Chemistry, 38, 133-166, Doi 10.1023/A:1006322701523, 2001.

Yang, Y. D., Shao, M., Wang, X. M., Nolscher, A. C., Kessel, S., Guenther, A., and Williams, J.: Towards a quantitative understanding of total OH reactivity: A review, Atmospheric Environment, 134, 147-161, 10.1016/j.atmosenv.2016.03.010, 2016.

Yang, Y. D., Shao, M., Kessel, S., Li, Y., Lu, K. D., Lu, S. H., Williams, J., Zhang, Y. H., Zeng, L. M., Noelscher, A. C., Wu, Y. S., Wang, X. M., and Zheng, J. Y.: How the OH reactivity affects the ozone production efficiency: case studies in Beijing and Heshan, China, Atmospheric Chemistry and Physics, 17, 7127-7142, 10.5194/acp-17-7127-2017, 2017.

Yuan, B., Warneke, C., Shao, M., and de Gouw, J. A.: Interpretation of volatile organic compound measurements by proton-transfer-reaction mass spectrometry over the deepwater horizon oil spill, International Journal of Mass Spectrometry, 358, 43-48, 10.1016/j.ijms.2013.11.006, 2014.

Zannoni, N., Gros, V., Esteve, R. S., Kalogridis, C., Michoud, V., Dusanter, S., Sauvage, S., Locoge, N., Colomb, A., and Bonsang, B.: Summertime OH reactivity from a receptor coastal site in the Mediterranean Basin, Atmospheric Chemistry and Physics, 17, 12645-12658, 2017.

Zhao, J., Zhang, R. Y., Fortner, E. C., and North, S. W.: Quantification of hydroxycarbonyls from OH-isoprene reactions, J Am Chem Soc, 126, 2686-2687, 10.1021/ja0386391, 2004.

Tables and Figures

Table 1. Description of instrument and measured parameters.

Instrument	**Parameters**	**Measurement Uncertainty (1σ) and lower level of detection limit**
Chemical Ionization Spectroscopy - Comparative Reactivity Method (CIMS-CRM)	OH reactivity	16.7% (5 sec-1)
Thermo Scientific 42i	NO	20% (100 ppt)
Cavity Ring Down Spectroscopy	NO_2	20% (50 ppt)
Thermo Scientific 49i	O_3	4% (1 ppb)
Lufft 501 C	Temperature	±0.3 °C (NA)
Thermo Scientific 48i TLE	CO	10% (50 ppb)

Thermo Scientific 43i TLE	SO_2	10% (100 ppt)
Mini Tunable Infrared Laser Direct Absorption Spectroscopy (mini-TILDAS) Formaldehyde Monitor(Herndon et al., 2005) (Aerodyne Research, Inc)	HCHO, CH_4, CH_3OH	5% (few tens ppt)
Proton Transfer Reaction Time of Flight Mass Spectrometer (PTR-TOF-MS 8000, IONICON Analytik, GmbH)	Acetaldehyde, Ethanol, Acetone, Isoprene, MVK + MACR, Methyl ethyl ketone, Benzene, Monoterpenes, Toluene, Furfural, Benzaldehyde, Xylenes, Trimethylbenzenes, Sesquiterpenes	Isoprene 9.8% Benzene 6.9% Toluene 6.5% Monoterpenes 9.2% Xylenes 4.0% Other 16.5% (tens ppt)

868

869

870

871

Figure 1. Observed and calculated OH reactivity during KORUS-AQ 2016. The measured and calculated OH reactivity are on the left axis while the missing OH reactivity is on the right axis. The yellow box represents the stagnation period and the blue box represents the transport period.

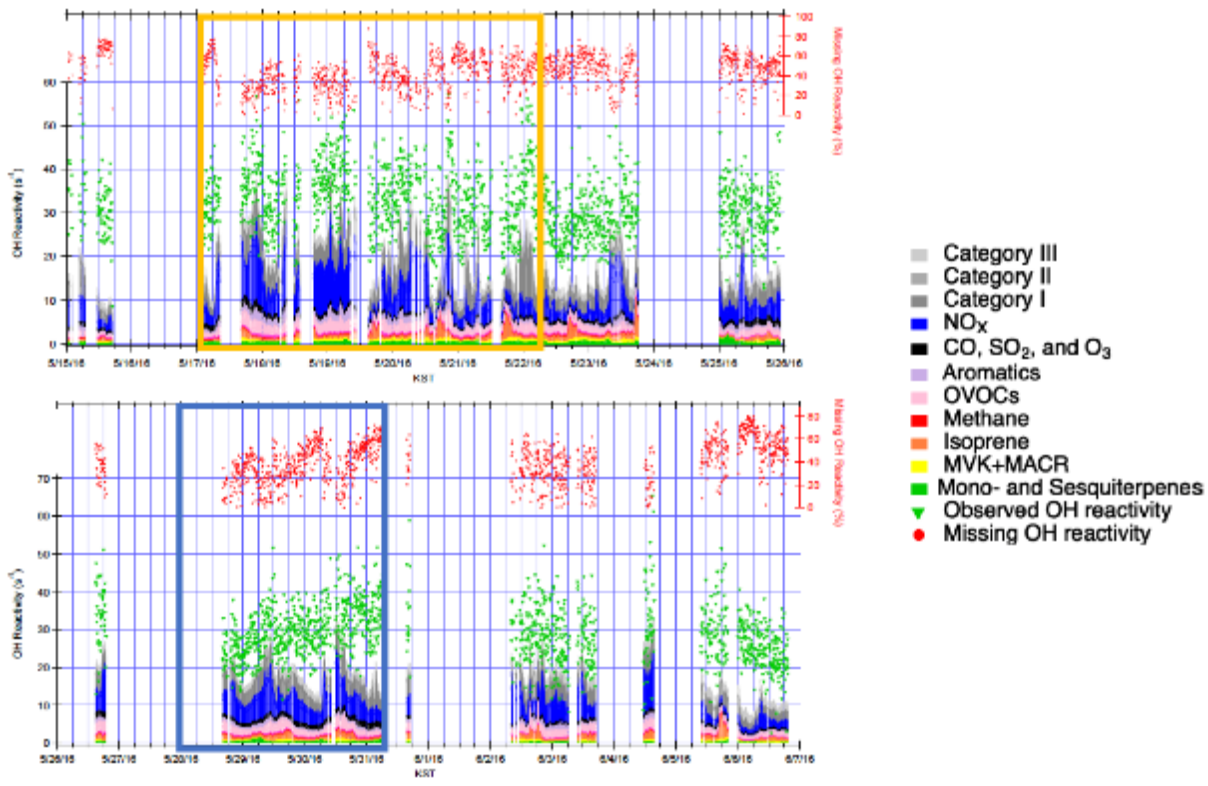

Figure 2. The diurnal average of OH reactivity from 15 May 2016 – 7 June 2016. The measured and calculated OH reactivity are on the left axis. The blue shading represents uncertainty in the measured OH reactivity. The black bars represent the propagated uncertainty of calculated OH reactivity. The missing OH Reactivity in the percentage scale can be read using the right axis.

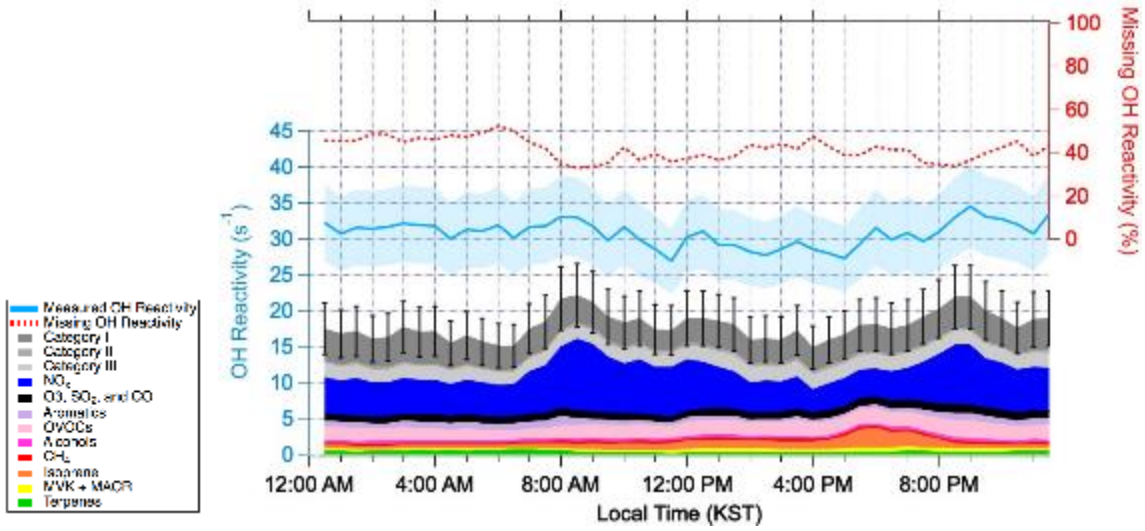

Figure 3. Diurnal averages of OH reactivity during the stagnation period (A) from May 17th – May 22nd in 2016 and the transport period (B) from 28 May – 1 June 2016. The measured and calculated OH reactivity are on the left. The blue shading represents an uncertainty of 16.7% at 1σ. The black bars represent the propagated uncertainty of 20.1% at 1σ from calculated missing OH reactivity. The percent missing OH reactivity is on the right axis.

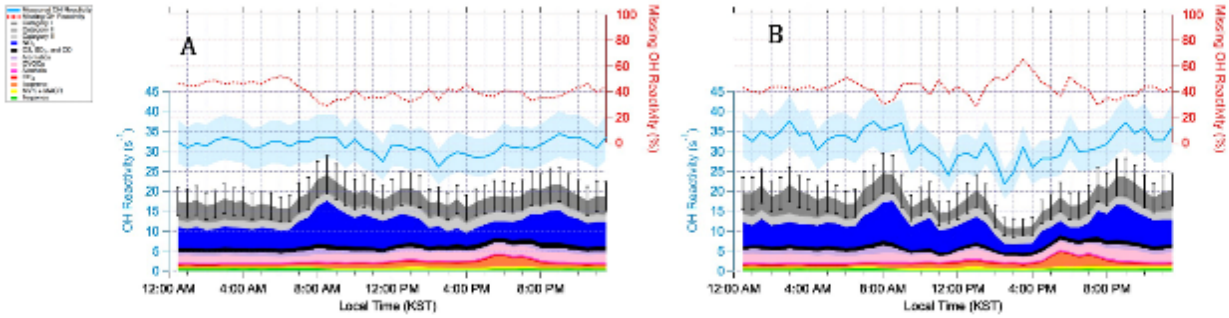

Figure 4. The observed OH reactivity during the overall campaign, stagnation period, and transport period.

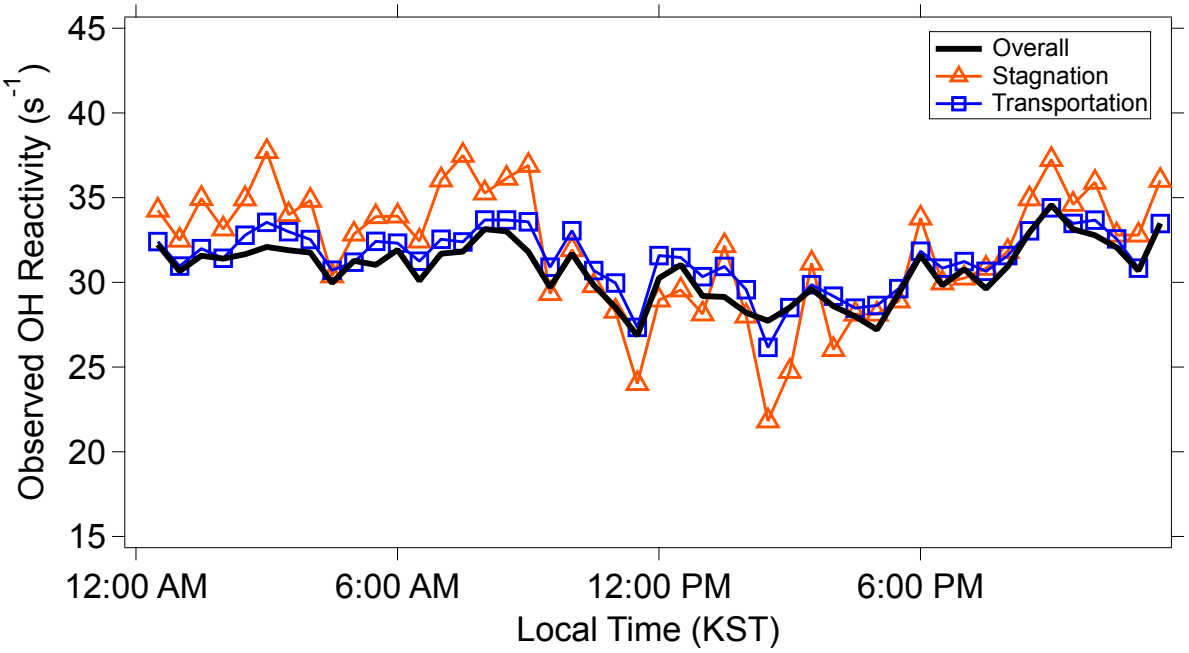

Figure 5. Diurnal profiles for different classes of trace gases during the different periods. A) criteria pollutants NO_x, O_3, SO_2, and CO B) Aromatics, C) BVOCs, and D) OVOCs

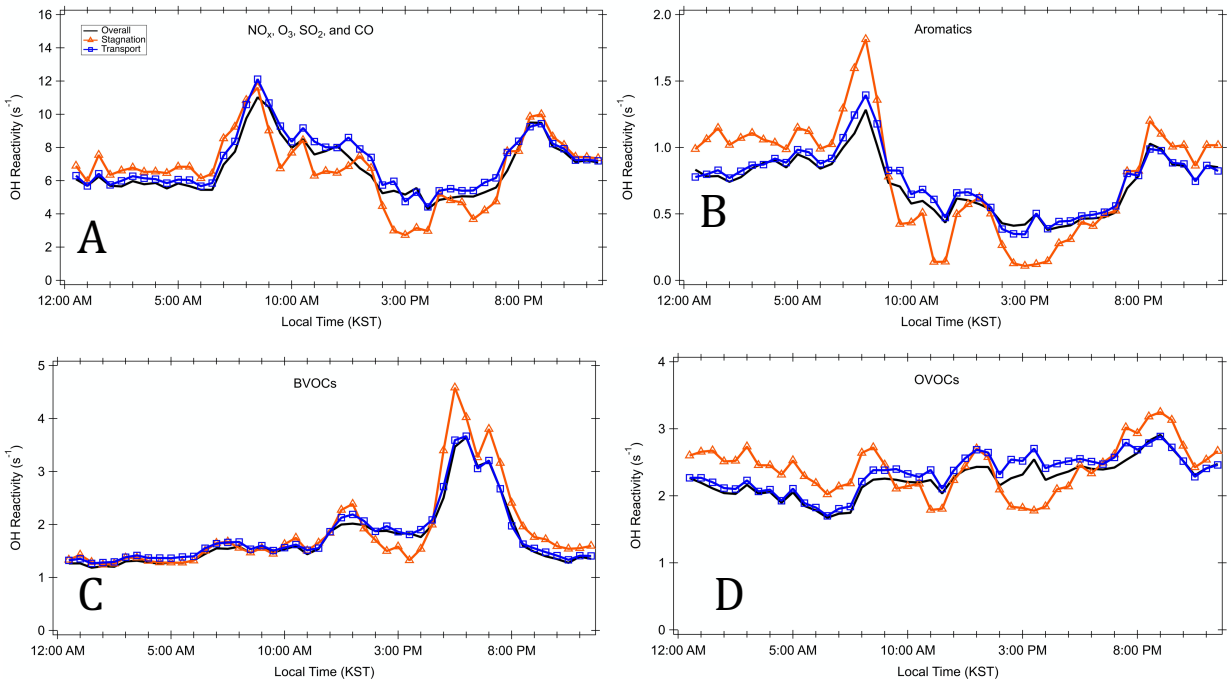

Figure 6. Diurnal averages of the OH reactivity from the compounds in A) Category I, B) Category II and C) Category III

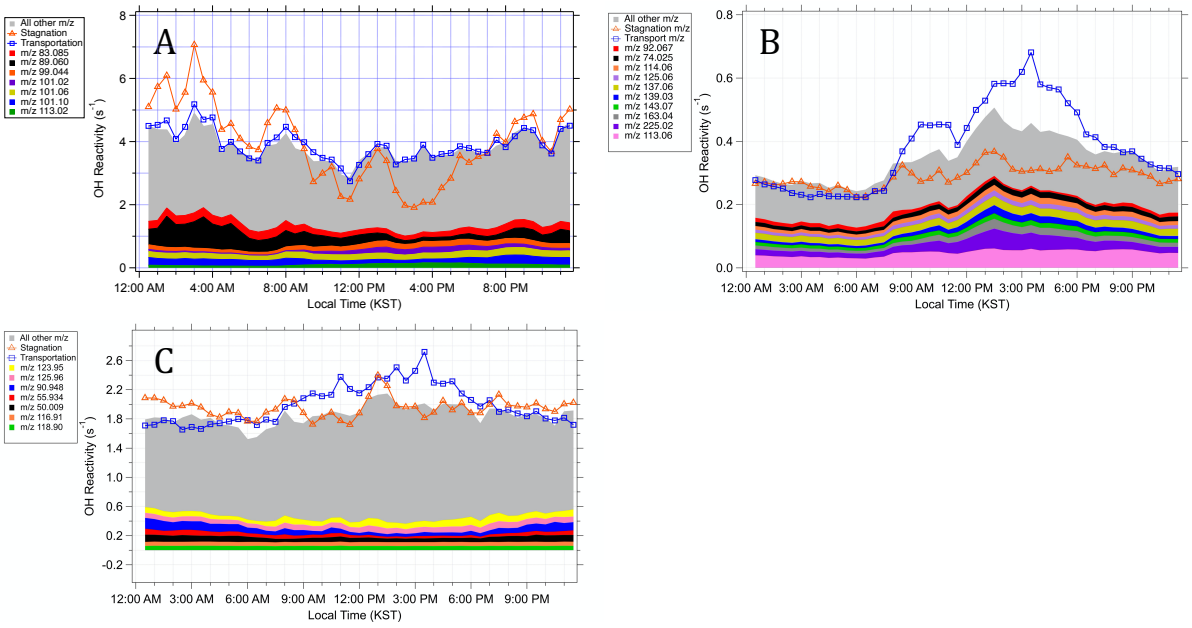

960 Figure 7. The correlation between A) NOx OH reactivity and absolute missing OH reactivity and

961 B) percent missing OH reactivity

962

963

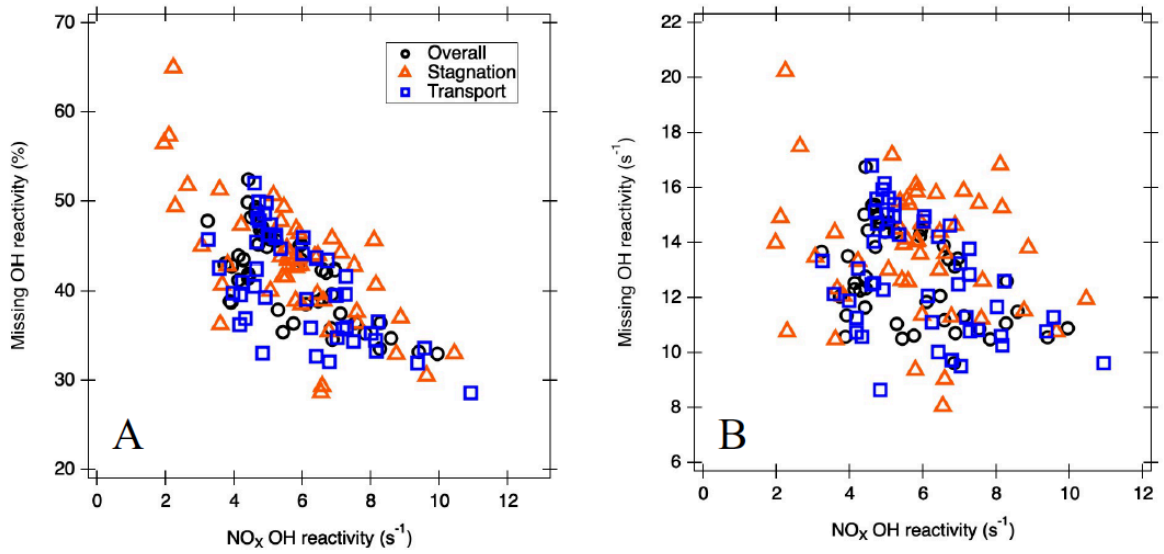

964